Int. J. Nano Dimens., 14 (2): 126-137, Spring 2023

ORIGINAL ARTICLE

Antibacterial activity of Fe-doped Cd_2SnO_4 nanoparticles against *staphylococcus aureus* and *salmonella typhi*

Alagu Lakshmi Alagarsamy[1], Pandiarajan Jeyaprakash[1], Mariappan Subramanian[2], Prithivikumaran Natarajan[1], Jeyakumaran Natarajan[1, *]

[1] Energy Physics Lab, Department of Physics, V.H.N.Senthikumara Nadar College (Autonomous), Virudhunagar – 626 001, Tamil Nadu, India
[2] PG & Research Department of Zoology, Yadhava College (Autonomous), Madurai – 625 014, Tamil Nadu, India
(1 &2 Affiliated to Madurai Kamaraj University, Madurai, Tamil Nadu, India)

Received 26 November 2022, revised 13 January 2023, accepted 23 January 2023, available 28 January 2023

Abstract

Metal oxide nanoparticles are capable of successfully inhibiting bacterial strains. Among the several transition metal atoms, iron (Fe) looks to be a viable dopant since iron oxide has been used a lot in biomedical research due to its biocompatibility and magnetic properties. In order to boost its antibacterial activity and facilitate the entry of nanoparticles into bacterial cells, Cd_2SnO_4 has been selectively doped with Fe. The chemical precipitation method was used to synthesize Cd_2SnO_4 and Fe-doped Cd_2SnO_4 nanoparticles for antibacterial activity. To the best of our knowledge, there is no report is available on the antibacterial activity of undoped and Fe-doped cadmium stannate nanoparticles against *salmonella typhi*. The nanoparticles formed are in the cubic phase, according to the XRD results, the size of the crystallites is seen to grow as the increase in Fe concentrations. By using the Well diffusion method, the antibacterial properties of synthesized nanoparticles were examined against two human pathogens, including *staphylococcus aureus* and *salmonella typhi*. Both undoped and Fe-doped Cd_2SnO_4 nanoparticles have antibacterial action that inhibits pathogen growth, according to antibacterial tests, which have shown the presence of a zone of clearing surrounding the well.

Keywords: *Cd_2SnO_4 Nanoparticles; Chemical Precipitation; Fe Doped; S.aureus; SEM; S.typhi; XRD.*

How to cite this article

Lakshmi Alagarsamy A., Jeyaprakash P., Subramanian M., Natarajan P., Natarajan J. Antibacterial activity of Fe-doped Cd_2SnO_4 nanoparticles against staphylococcus aureus and salmonella typhi. Int. J. Nano Dimens., 2023; 14(2): 126-137.

INTRODUCTION

A contemporary branch of study known as nanobiotechnology seeks the unique physical, chemical, and biological characteristics of nanostructures and their uses in a variety of industries, including agriculture and medicine [1]. Global public health is seriously threatened by the spread of infectious diseases in general, particularly by the rise of bacterial strains that are resistant to antibiotics. Gram-positive and Gram-negative bacterial strains are generally observed as serious public health issues [2]. Gram-negative bacteria called *salmonella typhi* (*s. typhi*) can infect both the blood and the digestive system. Milder illness of typhoid fever is caused by the *s. typhi* bacteria [3]. One of the most dangerous bacteria for humans is *staphylococcus aureus* (*s. aureus*). It can cause a wide range of illnesses in people, from basic, benign infections like boils, carbuncles, styes, and abscesses to some serious, fatal illnesses like sepsis, meningitis, and pneumonia [4].

Bacterial strains can be effectively inhibited by metal oxide nanoparticles. The antibacterial effectiveness of metal oxide nanoparticles is influenced by factors such as particle size, light exposure, aqueous medium composition, *etc*. Bacterial attachment of nanoparticles is caused

* Corresponding Author Email: *jeyakumaran@vhnsnc.edu.in*

by electrostatic interactions. As a result of these interactions, bacteria experience oxidative stress and changes in the integrity of their cell membranes. [5-7]. The creation of metal oxide nanoparticles that are stable enough to significantly restrict bacterial growth in the nutrient medium is very difficult.

Cadmium Stannate (Cd_2SnO_4) is an *n*-type semiconductor. The high charge carrier density ($\sim 10^{21}$ cm^{-3}), high mobility ($\sim$100 cm^2 $V^{-1}s^{-1}$) low visible light absorption and chemical stability are the special features of the materials. Various methods are used to synthesize Cd_2SnO_4 nanoparticles, such as solution combustion method, hydrothermal method, sol-gel method, solid-state reaction method and chemical precipitation method [8-13], *etc*. Iron (Fe) appears to be a promising dopant among the numerous transition metal atoms since iron oxide has been employed extensively in biomedical research because of its biocompatibility and magnetic characteristics [14]. Iron, a vital nutrient, is captured by siderophores made by bacteria. Due to this, Cd_2SnO_4 has been specifically doped with Fe to increase its antibacterial action and make it easier for nanoparticles to enter bacterial cells [15].

Therefore, in this work, undoped and Fe-doped Cd_2SnO_4 nanoparticles (NPs) are synthesized using a chemical precipitation process at different Fe concentrations (1%, 5%, and 10%). Systematic research is done on the structural, surface morphological, chemical, optical, and antibacterial characteristics. Undoped and Fe-doped Cd_2SnO_4 NPs have the ability to inhibit the growth of the two main human infections, gram-positive *staphylococcus aureus* and *salmonella typhi* (gram-negative bacteria). In this study, the antibacterial activity of Fe-doped Cd_2SnO_4 NPs was reported for the first time. To the best of our knowledge, there have not been many reports on the antibacterial activity against *salmonella typhi*. The findings demonstrated that the antibacterial activity increased with increasing Fe-dopant concentrations.

MATERIALS AND METHODS

Synthesis of cadmium stannate nanoparticles

Both undoped and Fe-doped Cd_2SnO_4 nanoparticles have been synthesized using the chemical precipitation approach. The following precursors were bought from Isochem Laboratories in India: Cd $(CH_3COO)_2.2H_2O$ (Cadmium Acetate Dihydrate), $SnCl_2.2H_2O$ (Tin Chloride Dihydrate), and $FeCl_3$ (Ferric Chloride). Separately, 100 ml of deionized water was used to dissolve 1M each of Cd $(CH_3COO)_2.2H_2O$ and $SnCl_2.2H_2O$ by stirring continuously for an hour. One weight percentage of ferric chloride was added and continuously stirred for an hour in 100 ml of deionized water. The three solutions were then aggressively combined for two hours, and 1 M KOH solution was then gradually added until a cloud colour mixer was attained. The precipitate was repeatedly rinsed with deionized water and then placed on a heating mantle until the dry powder was formed. The produced nanoparticles were annealed at 800°C for 1 hour to get the desired nanostructure. The same procedure was done with $FeCl_3$ at 5 and 10 weight percentages. Fig.1. represents a

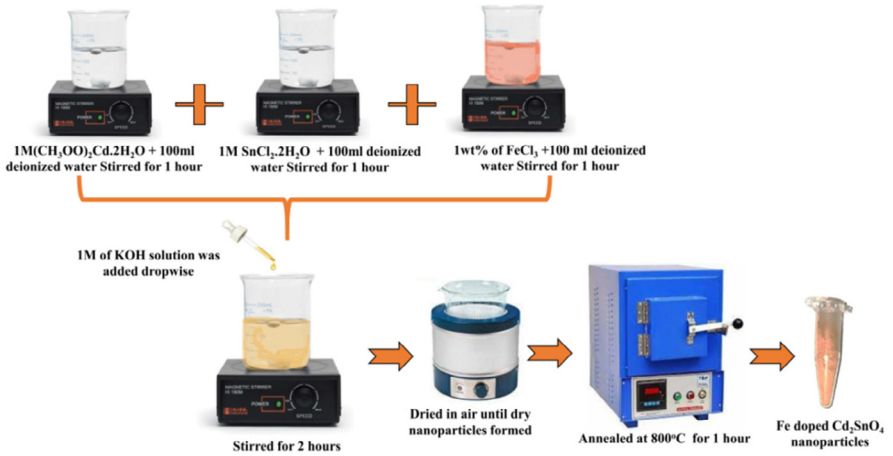

Fig. 1. Schematic representation for the synthesis of Fe-doped Cd_2SnO_4 NPs by chemical precipitation method.

Schematic representation for the synthesis of Fe-doped Cd_2SnO_4 NPs by the chemical precipitation method.

Characterization

Studies using the XRD, FESEM, EDAX, HR-TEM, UV-Visible, PL, FTIR, and XPS techniques were used to characterize the undoped and Fe-doped samples. The samples were recorded using a powder X-ray diffractometer (PANalytical X'Pert PRO) to assess the phase and crystallinity. The field emission scanning electron microscope was used to describe the nanoparticles' surface morphology (Carl Zeiss, SUPRA 55VP). High resolution transmission electron microscope imaging with SAED patterns was used to acquire crystal structure imaging of a sample at the atomic level (JEOL-2100 Plus). A Thermofisher Evaluation 220 spectrophotometer was used to evaluate the samples' UV-Visible absorption spectra. The Varian Cary Eclipse Spectroflurometer was used to capture photoluminescence emission spectra.

Evaluation of antibacterial activity

By using the well diffusion method, the antibacterial properties of nanomaterial were examined against two human pathogens, namely *salmonella typhi* (MTCC 733) and *staphylococcus aureus* (ATCC 700699). The Microbial Type Culture Collection (MTCC), Institute of Microbial Technology in Chandigarh, India, is where the human pathogenic microorganisms were collected. In Luria Bertani broth (LB), the pure bacterial culture was cultured for 24 hours at 37°C. On Muller-Hinton agar medium (MHA), undoped and Fe-doped Cd_2SnO_4 nanoparticles were examined for antibacterial activity using the agar well diffusion method at various doses, including 15, 20, 25, and 30 g/ml. In this investigation, erythromycin was utilized as a positive control. Using sterile buds and a sterile cork borer, the overnight human bacterial pathogens were swabbed onto MHA plates to create 9 mm diameter wells. Different concentrations of the nanomaterials and the negative controls were added to the agar well. At room temperature, the plates were incubated for 24 hours. The Petri plates were removed from the incubator after the incubation period had ended, and the diameters of the zones that had formed around the wells were measured and noted.

RESULTS AND DISCUSSION

XRD analysis

The XRD diffraction analysis is performed to analyse the effect of Fe dopant concentrations on the crystal phase and structural properties of undoped and Fe-doped Cd_2SnO_4 nanoparticles. Fig. 2(a) shows the XRD pattern of undoped and Fe-doped (1 wt%, 5 wt% and 10 wt%) Cd_2SnO_4 nanoparticles and Fig. 2(b) shows the JCPDS patterns. The XRD pattern shows the synthesized nanoparticles are crystalline in nature, which increases as the dopant concentration increases. The XRD pattern of the undoped Cd_2SnO_4 nanoparticles is in a mixed phase with the cubic

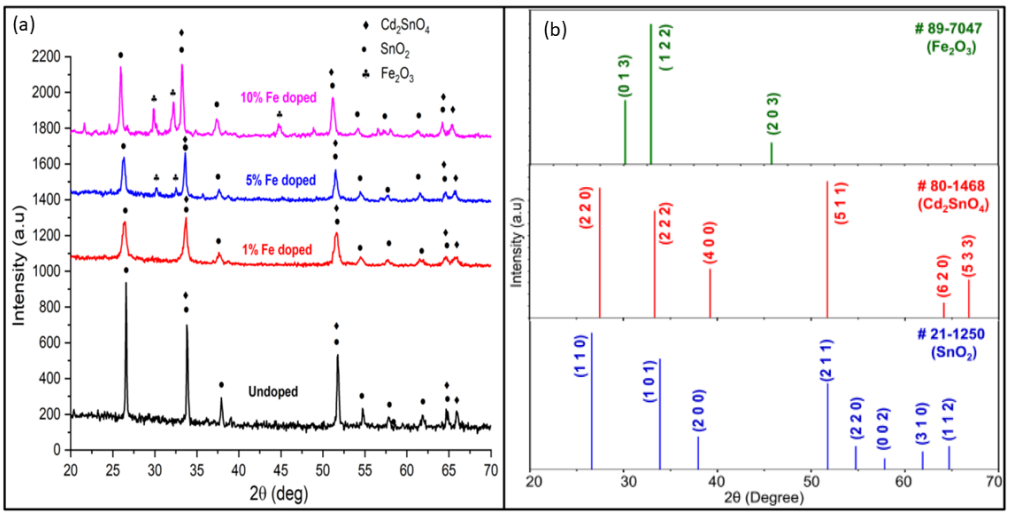

Fig. 2. XRD patterns of (a) undoped and Fe-doped (1 wt%, 5 wt% and 10 wt%) Cd_2SnO_4 nanoparticles (b) JCPDS patterns.

crystal structure. The peaks observed at 26.40º, 37.93º, 54.77º, 57.92º and 64.75° with (1 1 0), (2 0 0), (2 2 0), (0 0 2) and (1 1 2) planes of SnO_2 (JCPDS File No. #21-1250) [9]. The diffraction peak at 66.08º is associated with (5 3 3) plane of Cd_2SnO_4. The diffraction peaks at 33.88º and 51.83º be associated with the (2 2 2), (5 1 1) planes of Cd_2SnO_4 and/or possibly with the (1 0 1), (2 1 1) SnO_2 plane [16]. The sample at 1 wt% Fe concentration shows no change in their prominent peaks, which showed no change in the phase of the nanoparticles. The increase in FWHM and decrease in the intensity of the peaks confirm the incorporation of Fe^{3+} ions into Cd_2SnO_4 nanoparticles. The Fe doping concentration was increased to 5 wt% the additional low intense peaks are observed at 29.85º, 32.90º and 45.80º corresponding to (0 1 3), (1 2 2), (2 0 3) of Fe_2O_3. (JCPDS File No. # 89-7047).

Further, the doping concentration was increased to 10 wt% the intensity of the peaks corresponding to the Fe_2O_3 got increased. The FWHM values of all peaks were also reduced, confirming the increase in the crystalline nature of the nanoparticles [17].

The average crystallite size (D) of the Cd_2SnO_4 nanoparticles was calculated using the Debye–Scherrer's Eqn. (1) as:

$$D = \frac{k\lambda}{\beta \cos\theta} \quad (1)$$

Where *D, λ, k* and q are the average crystallite size, wavelength of radiation (1.5406 Å), constant (0.94), β full width at half maximum and q is Bragg's angle respectively. The dislocation density (δ) and microstrain (ε) were also determined using the Eqns. (2) & (3) as:

$$\delta = \frac{1}{D^2} \quad (2)$$

$$\varepsilon = \frac{\beta \cos\theta}{4} \quad (3)$$

From Fig. 3, it was found that the grain size increased with Fe dopant concentrations. Dislocation density and microstrain decrease with increasing Fe dopant concentrations. The various structural parameters calculated from XRD are presented in Table 1.

SEM with EDAX analysis

The SEM image of Fe-doped Cd_2SnO_4 nanoparticles shows the agglomerated particles' uneven distribution. With increasing Fe-dopant concentrations, the agglomeration rate rises even more. This increase in agglomeration is primarily attributable to the nanoparticle's higher surface free energy and larger surface area, which are more likely to agglomerate as a result of the stronger attractive forces that the surface atoms exhibit. [18]. With increasing doping concentration, the grain size and crystallinity of the Fe-doped Cd_2SnO_4 NPs increase, which is reliable with the findings of the XRD results. Fig. 4(a-c) shows

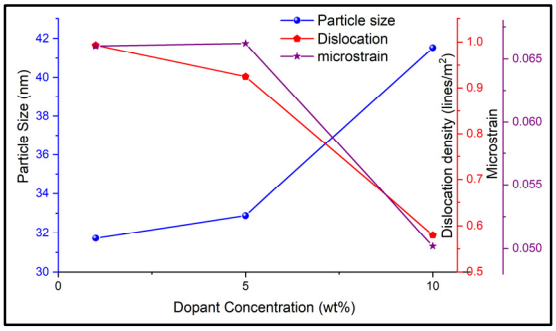

Fig.3. Doping concentrations *versus* particle size, dislocation density and microstrain of Fe doped Cd_2SnO_4 nanoparticles.

Table 1. Structural parameters of Fe doped Cd_2SnO_4 nanoparticles.

Fe dopant Concentration	Particle size (nm)	Dislocation density ($\times10^{15}$ lines/m^2)	Microstrain ($\times10^{-3}$)
1 %	31	0.99	0.067
5 %	33	0.92	0.066
10 %	42	0.58	0.050

the FESEM images of 1 wt%, 5 wt% , 10 wt% Fe doped Cd_2SnO_4 NPs. EDAX spectra matching Fig. 4(d) depiction of the components Cd, Sn, Fe, and O verified their presence as significant trace elements. The estimated percentage of weight was inserted in table.

HR-TEM analysis

The HR-TEM picture and lattice fringes of the 10 wt% Fe doped Cd_2SnO_4 nanoparticles are shown in Fig.5(a & b). As per the analysis done by ImageJ software, the lattice d spacing value of Fe-doped Cd_2SnO_4 is 0.354 nm, which represents the (2 2 0) plane of Cd_2SnO_4 and/or perhaps the (1 1 0) of SnO_2. Both the undoped and Fe-doped Cd_2SnO_4 NPs exhibit a cubic crystal structure, according to the SAED patterns seen from HR-TEM. The histogram of the particle size distribution that fits the Gaussian profile is shown in Fig. 5(c). It confirms that the particles are between 40 and 45 nanometers in size. The clear fringes in SAED patterns match the peaks seen in the XRD and the particle size quite well.

UV–Visible analysis

UV-visible spectrophotometer was used to examine the optical characteristics of undoped and Fe doped (1%, 5%, and 10%) Cd_2SnO_4 nanoparticles.

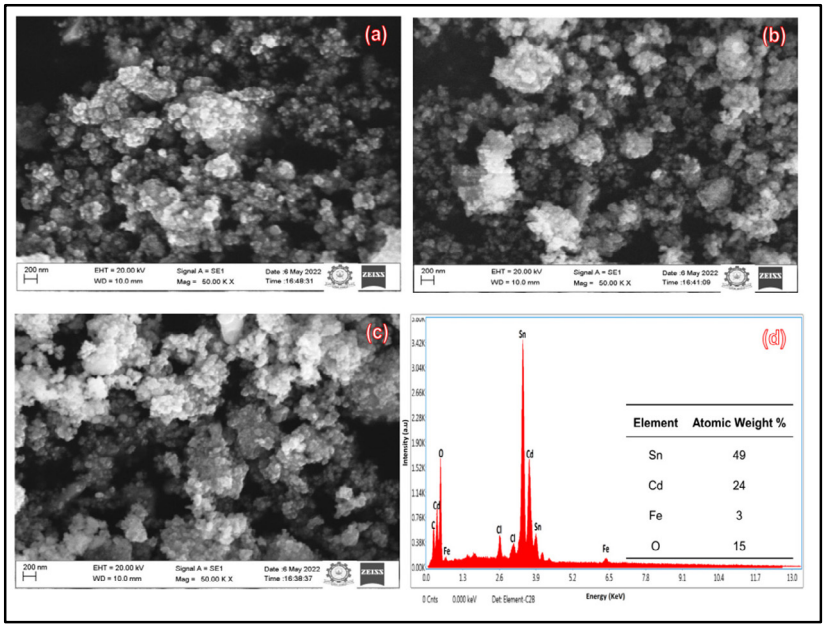

Fig. 4. FESEM images of (a) 1 wt% (b) 5 wt% and (c) 10 wt% Fe doped Cd_2SnO_4 NPs and (d) EDAX spectrum of 10 wt% Fe doped Cd_2SnO_4 NPs.

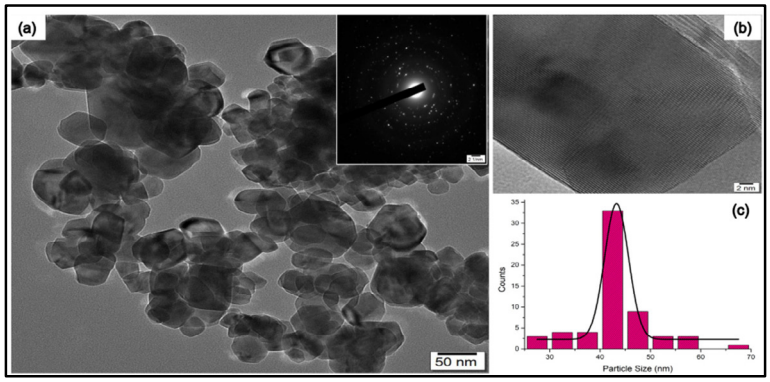

Fig. 5. (a & b) HR-TEM image (Inset: SAED pattern) (c) Particle size distribution plot with Gaussian fit of 10 wt% Fe doped Cd_2SnO_4 NPs.

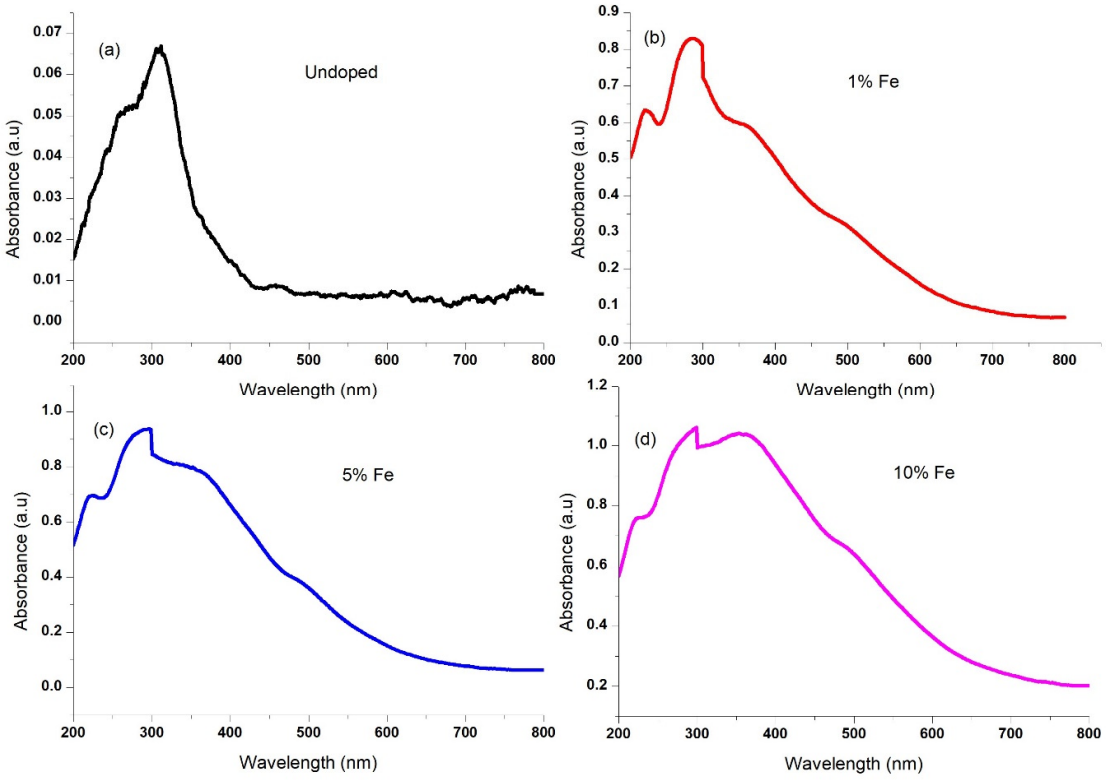

Fig. 6. Optical absorbance spectrum of (a) undoped and (b-d) Fe doped Cd_2SnO_4 NPs at various concentrations.

The absorption spectra of undoped and Fe-doped Cd_2SnO_4 nanoparticles are shown in Fig. 6(a-d). In order to raise the dopant concentrations, the absorption edge was in the visible area and then shifted to a higher wavelength side [19]. The reduction in the band gap of the Fe-doped Cd_2SnO_4 nanoparticles is indicated by the red shift of the absorption edge.

Tauc's formula is used to determine the optical absorption bandgap,

$$(\alpha hv) = A(hv - E_g)^n \quad (4)$$

Where α is the absorption coefficient, h is the Planck constant, ν is the frequency of the incident light, E_g is the energy band gap, and n is dependent on the type of transition occurring in the semiconductor. Since Cd_2SnO_4 is known to be a direct semiconductor for an authorised direct transition with n = 1/2 and for an indirect transition with n = 2.

Fig. 7(a-d), shows the Tauc's plot of undoped, 1%, 5%, and 10% Fe-doped Cd_2SnO_4 nanoparticles. By intersecting the extrapolated linear section with the (hv) on the X-axis, the optical bandgap (E_g) value is calculated to be 3.25 eV, 3.15 eV, 2.64 eV, and 2.42 eV from the graph [18]. The optical band gap was seen to narrow as the concentration of Fe-doping increased. The presence of the Fe in Cd-Sn metallic compounds may be the cause of the optical band gap lowering.

PL analysis

Using an excitation wavelength of 420 nm, Fig. 8 shows the PL emission spectra of undoped and Fe-doped Cd_2SnO_4 nanoparticles (1%, 5%, 10%). There are five different emission peaks in the visible region at wavelengths of 459 nm, 483 nm, 528 nm, 545 nm, and 573 nm, which correspond to blue, green, and yellow emissions, respectively, in the measured spectra of undoped and Fe-doped Cd_2SnO_4 nanoparticles [20]. As the concentration of Fe dopant increases, the emission peak diminishes. Combining holes from the valence band and electrons from the conduction band results in a peak at 459 nm. The electronic transitions from the top of the cadmium interstitials and oxygen vacancies could potentially

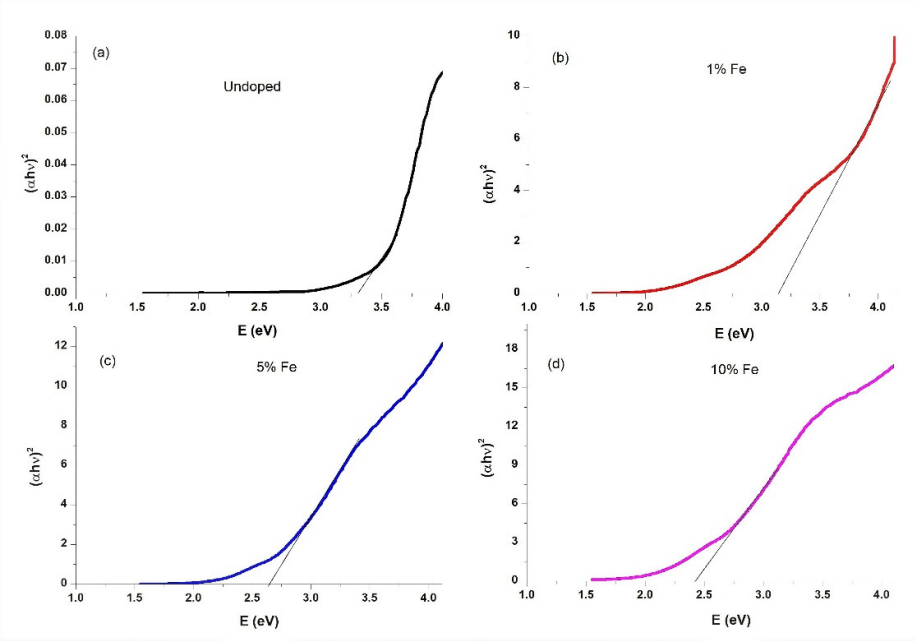

Fig. 7. Tauc's plot of the (a) undoped and (b-d) Fe doped Cd_2SnO_4 NPs at various concentrations.

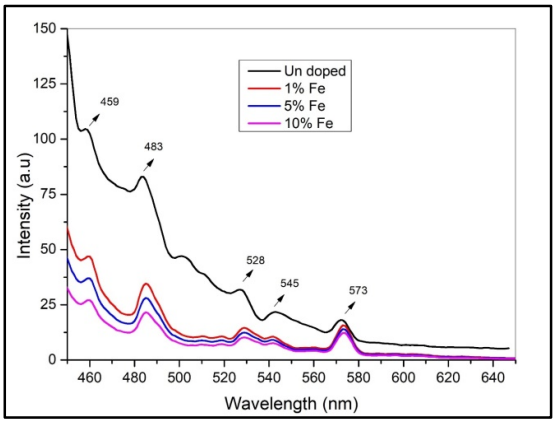

Fig. 8. PL emission spectra of the undoped and Fe doped Cd_2SnO_4 NPs.

be responsible for this peak [21]. Due to the near band edge emission of Cd_2SnO_4 nanoparticles, the nanoparticles showed a strong narrow emission band at 483 nm. The peak at 573 nm is associated with the dislocated luminescence centre, and the high-intensity green emission PL peak obtained at 528 nm relates to the recombination of holes with the ionised oxygen vacancies, known as a deep level of trap state emission [22]. Single oxygen vacancies were thought to be responsible for the green emission peak (545 nm) [23]. Additionally, the strength of the PL emission peak diminishes as the Fe concentration raises, showing that oxygen vacancies are capturing electron-hole pairs and producing singly ionised oxygen vacancies in the process [24].

FTIR analysis

Fe-doped and undoped Cd_2SnO_4 nanoparticles' FT-IR spectra were shown in Fig.9. The impact of the Fe dopant on the Cd_2SnO_4 lattice is what causes the intensity shifts in the vibrational modes of FTIR spectra. Stretching vibrations of O-Sn-O and Sn-O-Sn were attributed to the

vibrational modes between 400 and 850 cm^{-1} [25]. The production of Cd-O is confirmed by the absorption peak measured at 470 cm^{-1} [26]. The extra band with a centre at 1200 cm^{-1} is connected to the Cd-O stretching mode [27]. The stretching frequency of Fe-O was identified in the FT-IR transmission spectra of Fe_2O_3 oxide as the cause of the absorption bands at 470 and 610 cm^{-1} [15, 28]. The Sn-O vibration of the Sn-OH group and the stretching mode of O-Sn-O are attributed to the peaks found between 620 and 660 cm^{-1} [29].

The OH bending vibration of H_2O molecules is the cause of the peak seen near 1630 cm^{-1} [30]. The stretching vibrations of C-H are represented by the absorption peaks that occur at 2367 cm^{-1} and 2907 cm^{-1} [31]. The O-H stretching of the water molecules chemically linked to the metal results in a wide range from 3250 cm^{-1} to 3600 cm^{-1} [32]. The intensity of absorbed molecular water and the stretching mode of -OH both increase as the concentration of Fe increases [24].

XPS analysis

The elemental compositions of the material as well as the chemical and electronic states of the atoms have all been investigated using XPS analysis. The presence of Cd 3d, Sn 3d, Fe 2p, and O 1s elements is clearly visible in the XPS spectra

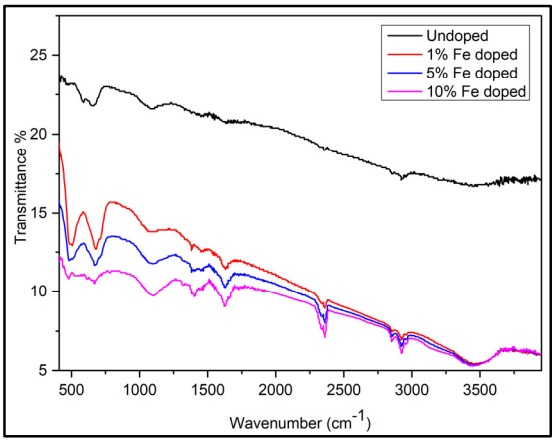

Fig. 9. FT-IR spectra of the undoped and Fe doped Cd_2SnO_4 NPs.

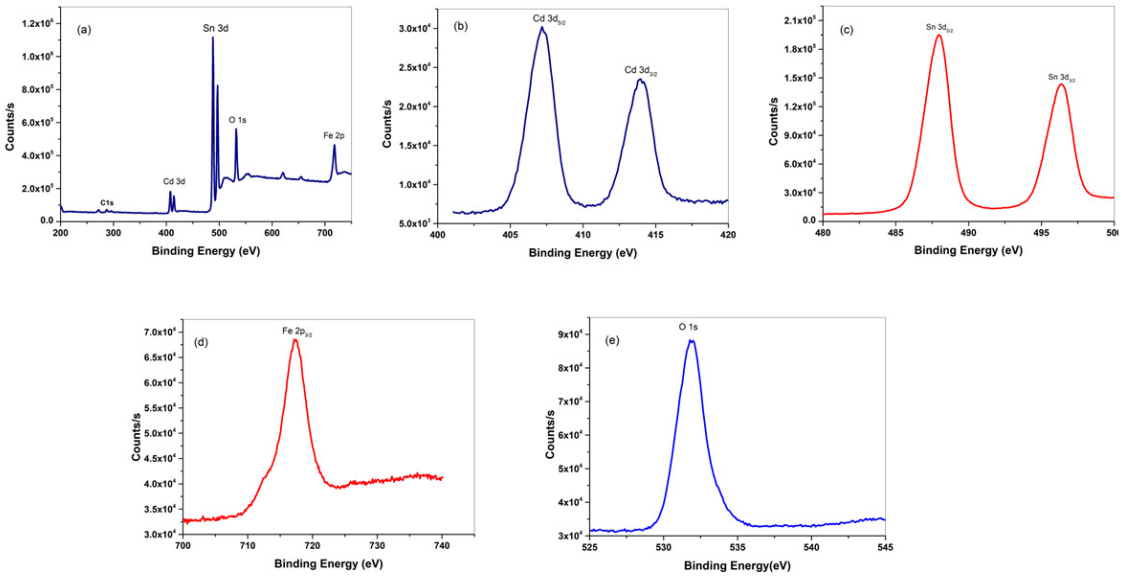

Fig. 10. (a) XPS survey spectra of Cd_2SnO_4 nanoparticles and XPS spectrum of (b) Cd 3d, (c) Sn 3d (d) Fe 2p and (e) O 1s elements.

(Fig. 10a) of cadmium stannate nanoparticles doped with 10% Fe. The presence of hydrocarbons in the instrument itself is what causes element C1s to exist. Fig. 10 (b-e) displays the XPS spectra of Cd 3d, Sn 3d, Fe 2p, and O 1s at high magnification. The spin orbitals Cd $3d_{5/2}$ and Cd $3d_{3/2}$ are allocated to the binding energy peaks at 406.6 eV and 413.4 eV, respectively, whereas the spin orbitals Sn $3d_{5/2}$, Sn $3d_{3/2}$ are responsible for the peaks at 487.3 eV and 495.7 eV. The peaks seen at binding energies of 717.3 eV are connected to Fe $2p_{3/2}$, which confirms that Fe is in the 3+ oxidation state [24]. The existence of adsorbed oxygen molecules in the corresponding cadmium stannate nanoparticles is related to the O $1s_{1/2}$ peak, which is observed at 531.2 eV [33]. These outcomes closely match the NIST XPS database.

Antimicrobial activity

By using the well diffusion method, the antibacterial effects of undoped and Fe-doped Cd_2SnO_4 nanoparticles were evaluated against two human pathogens, *staphylococcus aureus* (MTCC 700699) and *salmonella typhi* (MTCC 733). The positive control used was erythromycin. The results for the antibacterial activity of the different zones of inhibition (ZOI) against two human pathogenic microorganisms, including *staphylococcus aureus* and *salmonella typhi* , are shown in Fig. 11 (a) and 12 (a) show the control and Fig.11 (b, c) shows the zone of clearance surrounding the well-concentration dependent effect of undoped and 10 % Fe-doped Cd_2SnO_4 nanoparticles in comparison with antibiotics against *staphylococcus aureus*, and Fig.12 (b, c) shows the concentration-dependent effect of undoped and 10 % Fe doped Cd_2SnO_4 nanoparticles in comparison with antibiotics against *salmonella typhi* , suggests that the nanoparticles have antibacterial action that prevents the growth of pathogens. Nanoparticles' minimum inhibitory concentration (MIC) for infections is 15 g/ ml. But when compared to the positive control, undoped and Fe-doped Cd_2SnO_4 nanoparticles had a moderate amount of antibacterial activity against *salmonella typhi* and *staphylococcus aureus* at concentrations of 15 g/ml to 30 g/ml and 25 g/ml to 30 g/ml, respectively. Fe-doped Cd_2SnO_4 nanoparticles

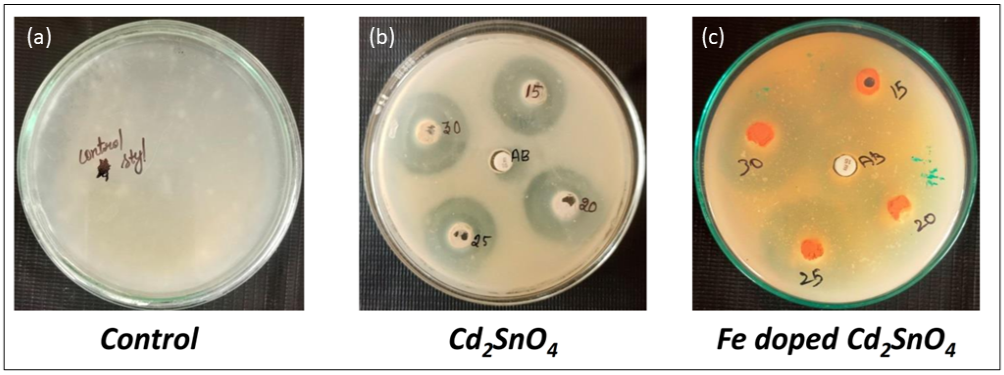

Fig. 11. (a) Control, concentration-dependent effect of (b) undoped and (c) Fe-doped (10%) Cd_2SnO_4 nanoparticles in comparison with antibiotics against *staphylococcus aureus.*

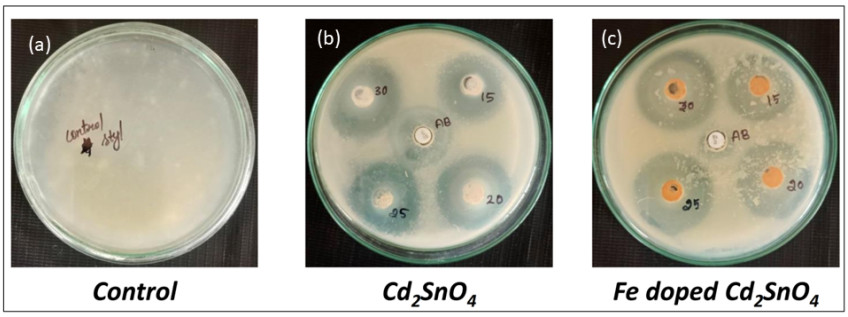

Fig. 12. (a) Control, concentration-dependent effect of (b) undoped and (c) Fe-doped (10%) Cd_2SnO_4 nanoparticles in comparison with antibiotics against *salmonella typhi.*

Table 2. Antimicrobial activity of undoped and Fe-doped Cd_2SnO_4 nanoparticles against *staphylococcus aureus.*

Samples	*staphylococcus aureus*			
	Concentrations			
	15 µg/ml	20 µg/ml	25 µg/ml	30 µg/ml
Undoped	10 mm	12 mm	13 mm	14 mm
Fe doped	15 mm	16 mm	19 mm	22 mm

Table 3. Antimicrobial activity of undoped and Fe-doped Cd_2SnO_4 nanoparticles against *Salmonella typhi* .

Samples	*salmonella typhi* .			
	Concentrations			
	15 µg/ml	20 µg/ml	25 µg/ml	30 µg/ml
Undoped	10 mm	12 mm	13 mm	14 mm
Fe doped	15 mm	16 mm	19 mm	22 mm

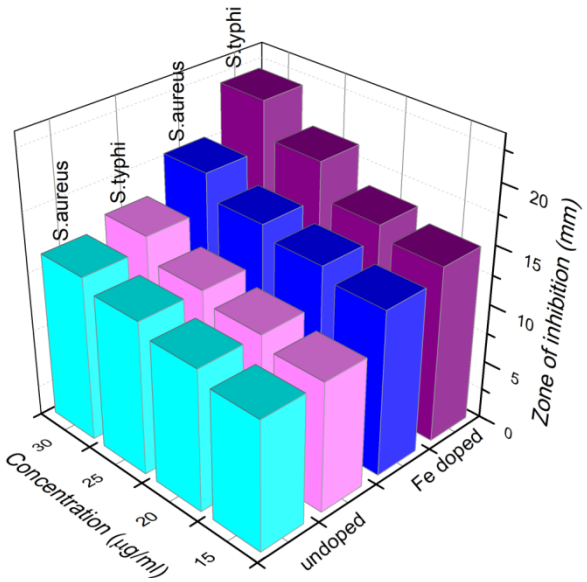

Fig. 13. Graphical presentation of antimicrobial activity against *staphylococcus aureus and salmonella typhi.*

showed the highest zone of inhibition for both *salmonella typhi* and *staphylococcus aureus* when compared to undoped Cd_2SnO_4 nanoparticles. This finding might also point to better Gram-positive strain resistance to or tolerance of Fe-doped nanoparticles compared to Gram-negative strains. Tables 2 and 3 show the inhibition zones. Antimicrobial activity against *salmonella typhi* and *staphylococcus aureus* is presented graphically in Fig. 13.

CONCLUSION

Chemical precipitation was used to successfully create undoped and Fe-doped Cd_2SnO_4 nanoparticles with varying Fe doping percentages (1wt%, 5Wt%, and 10Wt%). The cubic crystalline structure of both undoped and Fe-doped Cd_2SnO_4 nanoparticles is revealed by the XRD pattern. Images from a FESEM show that particle size increases as Fe concentrations rise. The particle size grew from 31 nm to 42 nm as the Fe content was raised. The cubic structure of the nanoparticles, which have a size of about 42 nm, is confirmed by HR-TEM investigation. With an increase in Fe concentration, there is an increase in UV absorption, and as dopant concentrations rise, the band gap value decreases from 3.15 eV to 2.42 eV. The presence of metal-oxide (M-O) bond is confirmed by the peak in the fingerprint area of the FTIR spectrum. It is closely

matched to the outcomes of the XRD analysis. The presence of Cd 3d, Sn 3d, Fe 2p, and O 1s elements is confirmed by XPS spectra. First tests on the antibacterial properties of undoped and Fe-doped Cd_2SnO_4 nanomaterial were conducted using the well diffusion method and two human pathogens, *staphylococcus aureus* and *salmonella typhi*. However, compared to the positive control (*Erythromycin*), undoped and Fe-doped Cd_2SnO_4 displayed a moderate level of antibacterial activity against *salmonella typhi* MTCC733 and *staphylococcus aureus* MTCC 700699. This study highlights the potential and effectiveness of both undoped and Fe-doped Cd_2SnO_4 nanoparticles as antibacterial agents for biomedical applications.

DECLARATIONS

Ethical Approval

Not applicable

Competing interests

The authors declare that they have no conflict of interest.

Funding

The authors declare that they have no financial or non-financial interests.

Authors' contributions

The author acknowledges B.L and N.P for general assistance, J.P.R for graphical design and Data analysis work. N.J for research supervision and validation of this work. The first author A. A thank Energy Physics Lab, Department of Physics, V.H.N.Senthikumara Nadar College (Autonomous), Virudhunagar, Tamil Nadu, India for providing Lab facilities.

Availability of data and materials

The present research results have not been published before. Data and Materials are all in the main text, figures and tables.

REFERENCES

1. Farnoush A., Zahra J., Mohammad I., Masoomeh S., Ghahfarokhi M., Razzaghi A., (2016), Antifungal nanomaterials: Synthesis, properties, and applications. *Nanobiomater. Antimicrob. Therapy.* 6: 343-383.
2. Ameer A., Arham S. A., Mohammad O., Mohammad S. K., Sami S. H., Adnan M., (2012), Antimicrobial activity of metal oxide nanoparticles against gram-positive and gram-negative bacteria: a comparative study. *Int. J. Nanomedic.* 7: 6003-6008.
3. Holland T. L., Arnold C., Fowler V. C., (2014), Clinical management of *staphylococcus aureus* bacteremia: A Review. *JAMA.* 312: 1330–1341.
4. Nancy J., Malu S., Nisha J. T., (2018), Characterization and anti–bacterial activities of SnO_2 nanoparticles using biological molecule. *IOP Conf. Ser.: Mater. Sci. Eng.* 360: 012007.
5. Nancy J., Malu S., Nisha J. T., (2017), Synthesis, characterization and anti - bacterial activities of pure an Ag-doped SnO_2 nanoparticles. *Mater. Today: Proceed.* 4**:** 4351–4357.
6. Bhattacharjee A., Ahmaruzzaman M., (2015), A novel and green process for the production of SnO_2 quantum dots and its application as a photocatalyst for the degradation of dyes from aqueous phase. J*. Colloid and Interf. Sci.* 448: 130-139.
7. Sarika A. K., Parvez A. S., Pradip P., Satishchandra B. O., (2012), Nanostructured Cd_2SnO_4 as an energy harvesting photoanode for solar water splitting. *Energy Environ. Sci*. 2: 5681-5685.
8. Wei W., Ying X., Xinyu Z., Bing L., Minhua C., (2014), Synthesis of Cd_2SnO_4–SnO_2 hybrid micro-cubes with enhanced electrochemical performance for lithium-ion batteries. *Cryst. Eng. Comm.* 16: 922-929.
9. Dinesh S., Anandan M., Premkumar V. K., Barathan S., Sivakumar G., Anandhan N., (2014), Photocatalytic and electrochemical performance of hydrothermally synthesized cubic Cd_2SnO_4 nanoparticles. *J. Mater. Sci. Eng. B.* 214: 37-45.
10. Jayachandran M., Subramanian B., Mary J. C., Lakshmanan A. S., (1994), Cd_2SnO_4-its sol-gel preparation and materials properties. *Bull. Mater. Sci.* 17: 989-997.
11. Xianli H., Jun L., Zhaosheng L., Zhigang Z., (2010), Electronic structure and visible-light-driven photocatalytic performance of Cd_2SnO_4. *J. Alloys Compd.* 507: 341-344.
12. Sawant V. S., Shinde S. S., Deokate R. J., Bhosale C. H., Chougule B. K., Rajpure K. Y., (2009), Effect of calcining temperature on electrical and dielectric properties of cadmium stannate panel. *Appl. Surf. Sci.* 255: 6675-6678.
13. Pabchanda S., Putpan J., Laopaiboon R., (2009), Preparation and Properties of Fe-doped SnO_2 Thin Films by Spray Pyrolysis Technique. *UBUSCI-Journal - Historical Articles.* 21-28.
14. Saleha S. A., Ibrahim A. A., Mohamed S. H., (2016), Structural and optical properties of nanostructured Fe-doped SnO_2. *Acta Physica Polonica A.* 129: 1220 -1225.
15. Osorio-R. D., Torres D. G., Márquez-M. J., Castanedo P. R., Aguilar-Frutis M. A., Zelaya Á. O., (2018), Cd_2SnO_4 thin films obtained by spray pyrolysis using RTA post deposition treatments. *J. Mater. Sci: Mater. Electronics.* 29: 20470-20475.
16. Deshraj M., Bharti S., Abhishek A., Mukhtiyar S., Bhatnagar M. C., (2020), Phase dependent selectivity shifting behavior of Cd_2SnO_4 nanoparticles based gas sensor towards volatile organic compounds (VOC) at low operating temperature. *J. Alloys and Comp.* 820: 153117.
17. Preethi T., Senthil K., Pachamuthu M. P., Balakrishnaraja R., Sundaravel B., Geetha N., Stefano B., (2022), Effect of Fe doping on photocatalytic dye-degradation and antibacterial activity of SnO_2 nanoparticles. *Hind. Adsorp. Sci. Tech.* Article ID 9334079.
18. Chikhale L. P., Shaikh F. I., Mulla I. S., Suryavanshi Chikhale S. S., (2017), Synthesis, structural and optical properties of Fe-doped nanocrystalline SnO_2. *J. Mater. Sci: Mater.*

Electron. 28: 12063-12069.
19. Sakthivel P., Murugan R., Asaithambi S., Karuppaiah M., Vijayaprasath G., Rajendran S., Hayakawa Y., Ravia G., (2018), Studies on optoelectronic properties of magnetron sputtered cadmium stannate (Cd_2SnO_4) thin film as alternate TCO material for solar cell applications. *Ceramic Int.* 44: 2529-2538.
20. Balamurugan S., Balu A. R., Usharani K., Suganya M., Anitha S., Prabha D., Ilangovan S., (2016), Synthesis of CdO nanopowders by a simple soft chemical method and evaluation of their antimicrobial activities. *Pacific Sci. Rev. A: Nat. Sci. Eng.* 18: 228-232.
21. Djurišić A. B., Leung Y. H., Tam K. H., Ding L., Ge W. K., Chen H. Y., Gwo S., (2006), Green, yellow and orange defect emission from ZnO nanostructures: Influence of excitation wavelength. *Appl. Phys. Lett.* 88:103107-103113.
22. Zhiren Q., Wong K. S., Mingmei W., Wenjiao L., Huifang X., (2004), Microcavity lasing behavior of oriented hexagonal ZnO nano whiskers grown by hydrothermal oxidation. *Appl. Phys. Lett.* 84: 2739 -2741.
23. Ameer Baig A. B., Vadamalar R., Ramya V., (2021), Synthesis and investigation of Fe doped SnO_2 nanoparticles for improved photocatalytic activity under visible light and antibacterial performances. *Mater. Tech.* 36: 623-628.
24. Hilal K., Şeyma K., Ali O. A., Hatem A., (2015), Structural properties of size-controlled SnO_2 nanopowders produced by sol–gel method. *Mat. Sci. Semicon. Proc.* 38: 404-412.
25. Karthik K., Dhanuskodi S., Gobinath C., Prabukumar S., Sivaramakrishnan S., (2019), Multifunctional properties of CdO nanostructures synthesised through the microwave-assisted hydrothermal method. *Mater. Res. Innov.* 23: 310-318.
26. Kaviyarasu K., Manikandan E., Paulraj P., Mohamed S. B., Kennedy J., (2014), One dimensional well-aligned CdO nanocrystal by solvothermal method. *J. Alloys and Comp.* 593: 67-70.
27. Saad M. Y., (2021), Engineering of visible light photocatalytic activity in SnO_2 nanoparticles: Cu^{2+}integrated Li^+, Y^{3+} or Zr^{4+} dopants optical materials. 116: 111077.
28. Srinivas K., Manjunath Raoan S., Venugopal Reddy P., (2011), Structural, electronic and magnetic properties of $S_{n0.95}N_{i0.05O2}$ nanorods. *Nanoscale*. 3: 642-653.
29. Ishpal R., (2015), Facial synthesis of hexagonal metal oxide nanoparticles for low temperature ammonia gas sensing applications. *RSC Adv.* 5: 4135-4142.
30. Shanmugam N., Sathya T., Viruthagiri G., Kalyanasundaram C., Gobi R., Ragupathy S., (2016), Photocatalytic degradation of brilliant green using undoped and Zn doped SnO_2 nanoparticles under sunlight irradiation. *Appl. Surf. Sci.* 360: 283-290.
31. Fanbin M., Wei W., Xiangnan C., Xiaoling X., Man J., Lu J., Yong W., Zuowan Z., (2016), Design of porous C@Fe_3O_4 hybrid nanotubes with excellent microwave absorption. Phys. *Chem. Chem. Phys.* 18: 2510-2516.
32. Pan P., Ping W., Zhengyang C., Jiajia Z., Yu H., Jingcheng X., Xianying W., (2022), Worm-like porous and defect-structured cadmium stannate photoanodes for enhanced solar water oxidation. *Nanoscale Adv.* 4: 1227-1232.